Probing the Structure-Property-Composition Relationship in Organic-Inorganic Tri-halide Perovskites

Julia L. Payne[1*], Chengsheng Ni[1], Jonathon R. Harwell[2], Lethy Krishnan Jagadamma[2], Calum McDonald[3], Davide Mariotti[3], Ifor D.W. Samuel[2], John T. S. Irvine[1]*

[1] *School of Chemistry, University of St Andrews, North Haugh, St Andrews, Fife, KY16 9ST, UK.* [2] *School of Physics and Astronomy, University of St Andrews, North Haugh, St Andrews, Fife, KY16 9SS. UK.* [3] *School of Engineering, Ulster University, Shore Road, Newtownabbey, Co. Antrim, BT37 0QB,UK*

Keywords: photovoltaics, $CH_3NH_3PbI_3$, perovskite solar cells, doping, non-stoichiometry

Abstract

Here, we have synthesised a range of samples, with the formula $(CH_3NH_3)_{1-2x}(H_3NC_2H_4NH_3)_xPbI_3$, with different levels of ethylenediammonium substitution to probe non-stoichiometry at the A-site of the perovskite. A single phase region was identified and is accompanied by a change in photophysical properties. The influence of aliovalent substitution with ethylenediammonium iodide results in a decrease in HOMO level from -5.31 eV for $x = 0$ to -5.88 eV for $x = 0.15$.

1. Introduction

The use of $CH_3NH_3PbI_3$ in a solar cell was first reported in 2009 with an efficiency of 3.81 %.[1] Since then, the performance of $CH_3NH_3PbI_3$ based materials in solar cells has improved dramatically, with the current best certified single absorber devices reaching 22.1%.[2] This has been due to optimisation of the chemical composition, the synthetic procedure, control of film morphology and optimisation of device architecture.[3-12] The exceptional properties of $CH_3NH_3PbI_3$ arise from several features, such as low recombination rates, long electron and hole diffusion lengths, high carrier mobility, and high absorption coefficients.[13-15]

Inorganic perovskite oxides are well known for their ability to accommodate vacancies on the cation or anion sites, but to date this has been under explored experimentally in organic-inorganic tri-halide perovskites. This is surprising, especially as vacancy-mediated ionic diffusion is thought to be one possible explanation for the hysteresis observed in organic-inorganic tri-halide perovskite solar cells. Therefore, the purpose of this work is to explore the possibility of creating cation non-stoichiometry and therefore vacancies on the cation site in organic-inorganic tri-halide perovskites by studying the $(CH_3NH_3)_{1-2x}(H_3NC_2H_4NH_3)_xPbI_3$

system and to tune the composition by substituting with an aliovalent cation. This offers us the possibility of probing the influence of cation vacancies on the hysteresis in photovoltaic devices in future work. The ethylene diammonium cation was used due to its small size in comparison to other diamines along with the stability of the cation itself.

$CH_3NH_3PbI_3$ adopts a perovskite related structure, ABX_3, where A = $CH_3NH_3^+$, B = Pb^{2+}, X = I^-. $CH_3NH_3PbI_3$ exhibits three perovskite related polymorphs with cubic, tetragonal and orthorhombic symmetry.[16, 17] The compositional flexibility of oxide perovskites has been known for years and this feature is also becoming apparent in organic-inorganic tri-halide perovskites. To date there have been many studies investigating isovalent substitution in organic-inorganic tri-halide perovskites, whereby an ion (or molecule) on the A, B or X site may be replaced by another ion or molecule of the same charge. To date, such substitutions have included on the A-site the formamidinium cation and Cs , on the B site Sn, Sr, Ca and Cd and on the anion site Cl, Br and $(BF_4)^-$.[18-25]

The ability to carry out such substitutions is a particularly attractive feature of organic-inorganic tri-halide perovskite materials as it enables the fine-tuning of the energy gap (and hence photovoltaic performance) within the perovskite absorber material. Hao *et al.* reported a tin organic-inorganic tri-halide perovskite, $CH_3NH_3SnI_3$ with a power conversion efficiency of 5.23%, and the efficiency could be tuned by replacing iodide ions with bromide and an optimum power conversion efficiency could be achieved for $CH_3NH_3SnIBr_2$ of 5.73%.[23] Seok *et al.* has recently studied the $(H_2NCHNH_2PbI_3)_{1-x}(CH_3NH_3PbBr_3)_x$ system.[4, 18] Interestingly, the best photovoltaic performance was obtained at intermediate compositions (x = 0.15) indicating that tailoring the composition is required to tune parameters such as band gap, absorption coefficient, and power conversion efficiency. One particularly notable feature of this work is that substituting $H_2NCHNH_2PbI_3$ with CH_3NH_3Br achieves the 3-dimensional perovskite like connectivity of lead iodide octahedra which is adopted in the high temperature phase of $H_2NCHNH_2PbI_3$, whereas pure $H_2NCHNH_2PbI_3$ does not adopt a perovskite structure at room temperature, but instead adopts a structure that consists of 1-dimensional chains of PbI_6 octahedra. Interestingly, only substituting $H_2NCHNH_2PbI_3$ with Br results in a two phase system at x = 0.15, whereas the same level of methylammonium substitution isolates a phase-pure perovskite. Grätzel *et al.* have recently carried out a systematic study over a large range of compositional space of the $(CH_3NH_3)_{1-x}(H_2NCHNH_2)_xPbI_{3-y}Br_y$ system.[19] A total of 49 compositions were studied through photoluminescence, powder X-ray diffraction, absorption, DFT and solar cell device

performance. This yielded an equation for estimating the band gap of the materials from the composition of the perovskite. Interestingly, changing the anion was shown to have a larger effect on the absorption than changing the cation. The maximum power conversion efficiency in this system was 20.7% for the $(H_2NCHNH_2)_{0.66}(CH_3NH_3)_{0.33}PbI_{2.5}Br_{0.5}$ composition.[19] Perovskites which exhibit a degree of compositional optimisation on both the anion and cation sites exhibit the current highest efficiencies for organic-inorganic tri-halide perovskite solar cells.[4] The ability to adjust the energy gap of the organic-inorganic tri-halide perovskites offers a great deal of opportunity for development when the perovskites are coupled with silicon, or another perovksite with a different band gap, in the bottom layer as a tandem solar cell.[20, 26]

Several authors have studied the influence of Cs substitution in formamidinium lead halides, $H_2NCHNH_2PbX_3$ (X=I or Br). [20, 21, 27] With low levels of Cs substitution ($x = 0.1$) the high temperature perovskite phase of $H_2NCHNH_2PbI_3$ may be stabilised to room temperature, offering a significant improvement on device performance, as the unsubstituted $H_2NCHNH_2PbI_3$ phase at room temperature does not possess the 3-dimensional connectivity of PbI_6 octahedra which usually possess better photovoltaic properties. Cs substitution results in a blue-shift of absorption and photoluminescence which is indicative of shifting the band gap to higher energies. Snaith *et al.* have recently found a band gap of 1.74 eV could be achieved for the composition $(H_2NCHNH_2)_{0.83}Cs_{0.17}Pb(I_{0.6}Br_{0.4})_3$, which is optimum for working in a tandem solar cell with Si, and this offers the possibility of achieving power conversion efficiencies above the Schockley Queisser limit for a single junction solar cell.[20] A recent paper by the Grätzel group has shown that even further tuning of the perovskite composition can lead to materials with good power conversion efficiencies.[28] In particular, in this recent work by Grätzel, the A-site of the perovskite was a mixture of three cations (Cs^+, $CH_3NH_3^+$ and $H_2NCHNH_2^+$) and this was coupled with the anion site being occupied by a mixture of iodine and bromine atoms.[28]

Although much of the focus of the research into organic-inorganic tri-halide perovskites has focused on perovskites with a 3-dimensional connectivity of lead halide octahedra, work by David Mitzi and co-workers has shown the plethora of interesting structural crystal chemistry in these organic-inorganic tri-halides and this work has recently been reviewed.[29] When organic amines or diamines with longer organic chains are used, 2-dimensional layered perovskites may form, and depending on the cation, the perovskite layers may adopt a staggered or eclipsed conformation.[29, 30] It is also interesting to note that the organic-

inorganic family of perovskites may also be extended to perovskites with more complex anions such as formates and dicyanometallates.[31, 32]

The hysteresis exhibited by organic-inorganic tri-halide perovskites has been widely discussed in the literature and several possible theories for the hysteresis have been proposed, one of which is ionic migration.[33-38] Aliovalent substitution with a cation of different charge can create vacancies in a crystal structure and this is a commonly used technique for increasing the ionic conductivity of inorganic perovskite oxides. Ionic migration in perovskite oxides has been widely studied and some examples of perovskite ionic conductors include the well-known lithium ion conductor, $Li_{3x}La_{2/3-x}\square_{1/3-2/x}TiO_3$ (where $\square$ = vacancy), which contains cation vacancies on the A-site, oxide conductors such as $La_{1-x}Sr_xGa_{1-y}Mg_yO_{3-z}\square_z$ (with vacancies on the anion site) and the lithium conducting Li_3OCl/Li_3OBr anti-perovskites.[39-41] Despite the ability of the perovskite structure to accommodate vacancies, this area remains under explored experimentally in the field of organic-inorganic tri-halide perovskites.

Vacancy creation and ionic migration in organic-inorganic tri-halide perovskites have been studied computationally by several groups, although aliovalent substitution remains unexplored. Eames *et al.* have recently calculated the activation energy for migration of $CH_3NH_3^+$, Pb^{2+} and I^- in $CH_3NH_3PbI_3$.[34] Iodide vacancies have the lowest barrier to migration (at 0.58 eV) and this activation energy is in good agreement with the activation energies for hysteresis measured experimentally.[34] In a recent combined DFT-experimental study, Grätzel *et al.*, have probed two different theories regarding the cause of the hysteresis: ferroelectricity and ion migration. By measuring the *J-V* curve over a range of different temperatures, an experimental activation energy was obtained which was in good agreement with computational work, suggesting ion migration was the key for the hysteresis.[42] In addition the activation energy was also sensitive to the halides used, providing support for the halide migration. [42]

Although calculations have shown that the formation of an iodide vacancy is facile, Walsh *et al.* have shown that there is a low energy of formation for Schottky defects in $CH_3NH_3PbI_3$.[43] The methylammonium iodide defect had the lowest energy of formation of the Schottky defects studied and the energy required for the formation of such defects is much lower than in oxide perovskites, with one explanation for this being the lower formal charge of the cation and anions sites in organic-inorganic tri-halide perovskites.[43]

Experimentally, ionic migration has also been probed in a recent impedance spectroscopy investigation was carried out by Maier *et al.*.[44] This showed that $CH_3NH_3PbI_3$ is a mixed ionic-electronic conductor and that iodide conductivity was possible. The mixed formamidium-methylammonium lead iodide were also mixed conductors. A recent study by Snaith *et al*. has shown facile cation exchange between the methylammonium lead iodide and formamidinium lead iodide perovskites.[45] By simply dipping a film of $CH_3NH_3PbI_3$ into a solution of fomamidnium iodide, the methylammonium cations were gradually shown to be replaced by formamidnium cations, leading to the formation of $H_2NCNH_2PbI_3$. The reverse process could also be observed. This experimental evidence supports the theory of cation migration in $CH_3NH_3PbI_3$ which so far has remained understudied experimentally. Zhou *et al*. have also studied cation exchange at elevated temperature, forming $H_2NCHNH_2PbI_3$ from NH_4PbI_3 through the reaction with formamidinium acetate.[46]

We note that whilst preparing this manuscript, we have become aware of some related work on tin iodide perovskites which also use ethylenediammonium as a cation.[47-49] Although there are some similarities with the our work, there are still differences, in terms of the chemical compositions explored, photoluminescence and film morphology.[47]

Therefore, the aim of our work was to explore the effect of compositionally adjusting $CH_3NH_3PbI_3$ and to probe the non-stochiometry in organic inorganic tri-halide perovskites, by studying the $(CH_3NH_3)_{1-2x}(H_3NC_2H_4NH_3)_xPbI_3$ system and to probe how this influences the physical properties of the materials.

2. Results and Discussion

$(CH_3NH_3)_{1-2x}(H_3NC_2H_4NH_3)_xPbI_3$ samples were synthesised with x = 0 to 0.5 using a procedure based on the method reported by Poglitsch *et al.*[50] for $CH_3NH_3PbX_3$ halides. With increasing ethylenediamine content, there was a gradual colour change, from black for the $CH_3NH_3PbI_3$ rich members ($x < 0.15$), to red and finally to yellow for the x = 0.5 sample. The change in colour with ethylenediammonium content is shown in Figure 1 for the ethylenediammonium rich samples, with the x = 0.25 sample being red and the x = 0.5 sample being yellow in colour.

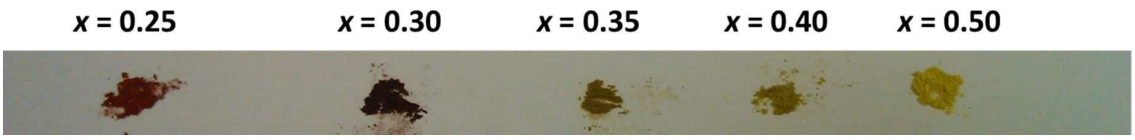

Figure 1: Change in colour of $(CH_3NH_3)_{1-2x}(H_3NC_2H_4NH_3)_xPbI_3$ with increasing ethylenediammonium content.

Ultraviolet-visible absorption data were collected on the $CH_3NH_3PbI_3$-rich thin films and this is shown in Figure 2. Here the absorption is shifted to lower wavelengths as the amount of $(H_3NC_2H_4NH_3)^{2+}$ increases, with the $x = 0$ sample showing an absorption onset of 764 nm and the $x = 0.15$ sample showing an absorption onset of 740 nm. The band gap was estimated from a Tauc plot (see Figure S1 and S2) and these values are indicated in Table 1. As can be seen from Table 1, the band gap increases with $(H_3NC_2H_4NH_3)^{2+}$ content, from 1.59 eV for $x = 0$ to 1.67 eV for $x = 0.15$.

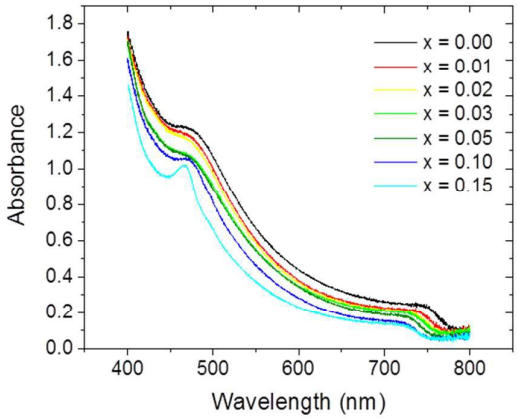

Figure 2: Absorption data for the $(CH_3NH_3)_{1-2x}(H_3NC_2H_4NH_3)_xPbI_3$ system

Table 1: Change in band gap for the $(CH_3NH_3)_{1-2x}(H_3NC_2H_4NH_3)_xPbI_3$ system, as determined from a Tauc plot of the absorption data.

x in $(CH_3NH_3)_{1-2x}(H_3NC_2H_4NH_3)_xPbI_3$	Band gap (eV) estimated from Tauc plot
0	1.59
0.01	1.61
0.02	1.62
0.03	1.63
0.05	1.65
0.10	1.67
0.15	1.67

The phase purity of the $(CH_3NH_3)_{1-2x}(H_3NC_2H_4NH_3)_xPbI_3$ bulk samples were monitored with powder XRD. Figure 3 shows the powder XRD patterns for bulk samples with x = 0 to 0.5. Clear changes in the diffraction pattern were observed upon increasing ethylenediamine content. Between x = 0 and 0.1, all peaks could be indexed to the parent tetragonal unit cell (*I*4/*mcm*, a = 8.87231(16) Å, c = 12.6637(2) Å for x = 0) and no peaks corresponding to PbI_2 (which is a common impurity in these systems) could be observed. For x > 0.1 to x = 0.15, a cubic structure is adopted and for x > 0.2 two phases are clearly observed in the diffraction patterns.

Figure 4 shows the evolution of cell volume with increasing ethylenediammonium content. At low substitution levels the cell volume only shows a small increase with increasing $(H_3NC_2H_4NH_3)^{2+}$ content. At higher substitution levels when a cubic structure is adopted, the cell volume increases, as expected, given the larger size of $(H_3NC_2H_4NH_3)^{2+}$ with respect to $CH_3NH_3^+$. Increasing the $(H_3NC_2H_4NH_3)^{2+}$ content further resulted in a two phase region. The synthesis of phase pure materials in the region x = 0 to 0.15 and the evolution of cell parameters with increasing ethylenediammonium indicate a region of solid solution. This behaviour and the dependence of the cell volume provide evidence for the substitution mechanism whereby two methylammonium cations are replaced by one ethylenediammonium cations and one vacancy on the A-site.

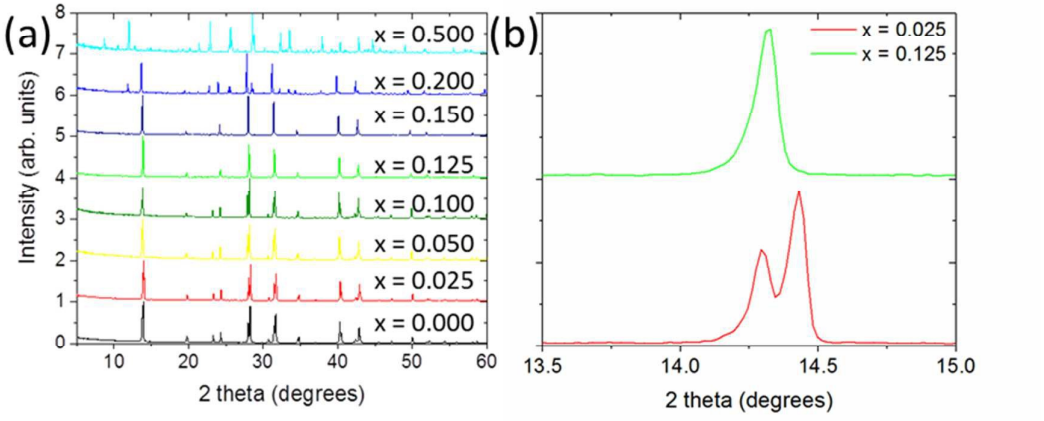

Figure 3: (a) Evolution of diffraction pattern with ethylenediammonium content in the $(CH_3NH_3)_{1-2x}(H_3NC_2H_4NH_3)_xPbI_3$ system (b) zoomed section of diffraction patterns for x = 0.025 (tetragonal) and x = 0.125 (cubic) showing change in crystal structure from tetragonal to cubic.

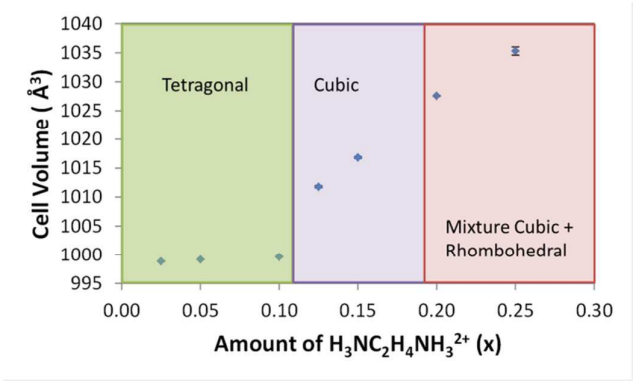

Figure 4: Variation of perovskite unit cell volume for $(CH_3NH_3)_{1-2x}(H_3NC_2H_4NH_3)_xPbI_3$

As X-ray diffraction is dominated by Pb and I containing phases, elemental analysis was carried out to confirm the CHN content in the materials. The C:H:N ratios for the bulk samples are given in Table 2. The elemental analysis showed a higher percentage of C, H and N than expected for samples close to the $x = 0.5$ end member. Calculations indicate that these values are consistent with the formation of $H_3NC_2H_4NH_3PbI_4$ as the '$x = 0.5$' end member. In the two phase region $(CH_3NH_3)_{1-2x}(H_3NC_2H_4NH_3)_xPbI_3$ coexists with the new material, $H_3NC_2H_4NH_3PbI_4$, before a single phase region based on $H_3NC_2H_4NH_3PbI_4$ is observed. We have studied the structure and properties of $H_3NC_2H_4NH_3PbI_4$ and this will be reported in a separate publication.[51]

Table 2: Elemental analysis results for $(CH_3NH_3)_{1-2x}(H_3NC_2H_4NH_3)_xPbI_3$ samples

	Experimentally determined values			Theoretically calculated		
x	% C	% H	% N	% C	% H	%N
0	2.06	0.86	2.36	1.94	0.98	2.26
0.025	2.02	0.87	2.33	1.94	0.96	2.26
0.100	1.98	0.88	2.33	1.94	0.94	2.26
0.150	2.12	1.02	2.39	1.94	0.93	2.26
0.200	2.71	1.24	3.11	Mixed phase		
0.250	3.00	1.36	3.40	Mixed phase		
0.350	3.17	1.43	3.49	Mixed phase		
0.400	3.15	1.37	3.58	Mixed phase		
0.500	3.22	1.45	3.57	3.09	1.30	3.61

Density measurements carried out using Helium Pycnometry show a decrease in density with increasing ethylenediammonium content. In the $(CH_3NH_3)_{1-2x}(H_3NC_2H_4NH_3)_xPbI_3$ system, the density of $CH_3NH_3PbI_3$ was found to be 4.1729(22) g cm^{-3} and for x = 0.15 the density was found to be 4.0106(40) g cm^{-3}. This is in-line with the expected decrease in density due to the increasing unit cell volume.

There are several difficulties which preclude further characterisation of these materials in terms of vacancy content. Refinement of site occupancies from powder diffraction techniques would require the use of neutron diffraction using a deuterated sample and the extensive A-site positional/dynamical disorder for the cation alone prevents determination of the cation content from powder diffraction.

The photophysical properties of these samples were investigated on fabricated thin film. Figure 5 shows the SEM images obtained for the film of $CH_3NH_3PbI_3$ (x = 0) and the x = 0.1 sample of $(CH_3NH_3)_{1-2x}(H_3NC_2H_4NH_3)_xPbI_3$. A good film coverage was obtained for both the x = 0 and 0.1 samples. One noticeable difference between the films is that the sample substituted with ethylenediammonium exhibits a smaller grain size. Cation substitution has previously been shown to influence the film morphology in $CH_3NH_3Pb_{0.9}M_{0.1}I_3$ (where M = Sn, Sr, Ca and Cd) and $(FAPbI_3)_{1-x}(MAPbBr_3)_x$ (where x = 0 to 0.15), and was dependent on the nature of the cation used.[4, 24]

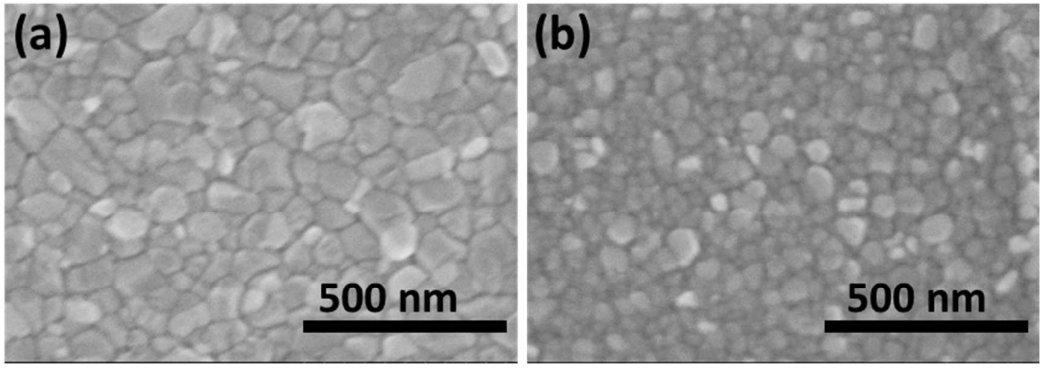

Figure 5: SEM images of films of $(CH_3NH_3)_{1-2x}(H_3NC_2H_4NH_3)_xPbI_3$ (a) x = 0 ($CH_3NH_3PbI_3$) and (b) x = 0.10

Photoluminescence measurements were carried out on thin films of the samples (x = 0 to 0.15). The photoluminescence (shown in Figure 6a) showed a gradual blue-shift with increasing ethylenediammonium content, from ~773 nm for $CH_3NH_3PbI_3$ to ~745 nm for x = 0.15. At higher ethylenediammonium contents the photoluminescence intensity gradually decreased, as the two phase region is approached. It is interesting to note that the blue-shift

in absorption and photoluminescence occur in other cation substituted organic-inorganic tri-halide perovskites. For example Seok *et al.* have observed similar trends in the $(H_2NCHNH_2PbI_3)_{1-x}(CH_3NH_3PbBr_3)_x$ system, with isovalent substiution on both the A and X sites.[4]

Air photoemission spectroscopy was used to determine the positions of the HOMO of the $(CH_3NH_3)_{1-2x}(H_3NC_2H_4NH_3)_xPbI_3$ materials and the position of these are indicated schematically in Figure 6b. It should be noted that these measurements were done on clean films, but in devices the band energies may change at the interface. The HOMO for $CH_3NH_3PbI_3$ was found to be -5.31 ±0.1 eV, which is close to other reported literature values of -5.39 eV and -5.40 eV for this material determined using UPS.[52, 53] On substituting with $(H_3NC_2H_4NH_3)^{2+}$, the HOMO decreased to -5.67 ±0.1 eV for the x = 0.05 sample and -5.91 ±0.1 eV for the x = 0.10 sample. Increasing the $(H_3NC_2H_4NH_3)^{2+}$ content further to x = 0.15 resulted in a HOMO level of -5.88 ±0.1 eV. This suggests that the limit of $(H_3NC_2H_4NH_3)^{2+}$ substitution has been reached and is close to the two phase region observed in powder X-ray diffraction patterns for the bulk materials.

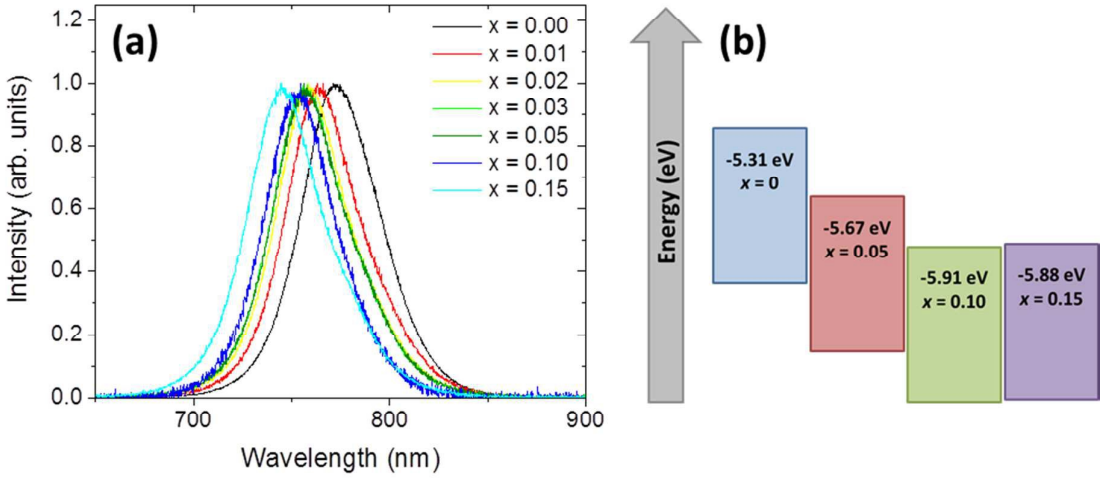

Figure 6: (a) Photoluminescence measurements and (b) schematic to show the change in HOMO level (as obtained from air photoemission spectroscopy) in $(CH_3NH_3)_{1-2x}(H_3NC_2H_4NH_3)_xPbI_3$

Trends in photoluminescence and absorption can also be plotted as a function of composition and these are shown in Figure 7a and b. The plot of the position of the photoluminescence maxima versus $(H_3NC_2H_4NH_3)^{2+}$ content is shown in Figure 7a. Here, the position of the photoluminescence maxima decreases with $(H_3NC_2H_4NH_3)^{2+}$ content and

there is a change in slope between $x = 0.03$ and 0.05. However, the position of the photoluminescence maxima continues to decrease, even for the $x = 0.15$ sample, rather than levelling off. As can be seen in Figure 7b, the absorption onset gradually decreases in wavelength as the $(H_3NC_2H_4NH_3)^{2+}$ content increases, with a change in slope being observed for samples above $x = 0.03$. This behaviour is similar to the changes in photoluminescence maxima with composition. However, at $x = 0.15$ the absorption onset remains very close to the value obtained for the $x = 0.10$ sample, indicating that the substitution limit has been reached.

From the evolution of cell parameters, absorbance, photoluminescence and air photoemission measurements, it can be seen that aliovalent substitution with $(H_3NC_2H_4NH_3)^{2+}$ tunes the electronic structure of the perovskite. A recently reported study on the $(H_2NCHNH_2)_{1-x}(CH_3NH_3)_xPbI_{3-y}Br_y$ system shows a correlation between cubic lattice parameter and band gap or photoluminescence.[19] In this case, the larger cell parameter indicated a smaller band gap.[19] However, it has been noted that the band-gap is not always a simple function of lattice parameter and deviations from Vegard's law and anomalous trends in band gap have been observed for mixed Pb-Sn perovskites.[22] DFT studies on the band structure of organic-inorganic tri-halides have shown several interesting factors which influence the band gap and the band structure of these materials.[54-57] These include the degree of octahedral tilting (and as a result Pb-halide-Pb bond angle), hydrogen bonding and spin orbit coupling.[54-57] These factors are expected to play a roll in the $(CH_3NH_3)_{1-2x}(H_3NC_2H_4NH_3)_xPbI_3$ system to differing extents and by replacing two $CH_3NH_3^+$ with one $(H_2NC_2H_4NH_2)^{2+}$ and a vacancy, the hydrogen bonding in the perovskite will be disrupted on a local scale.

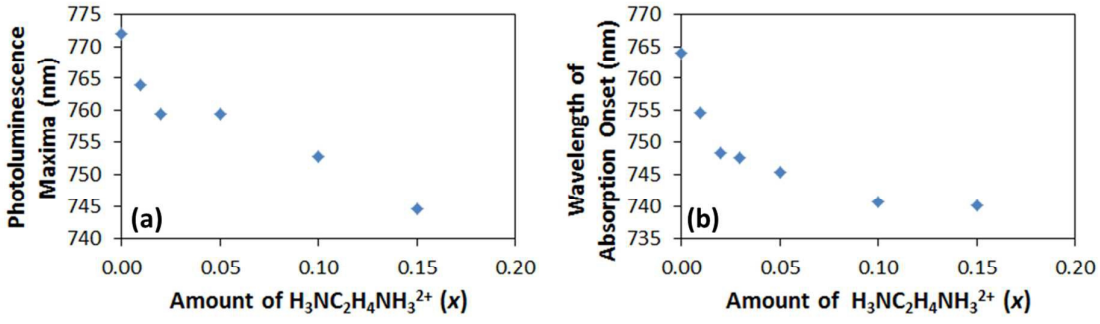

Figure 7: Evolution of (a) photoluminescence maxima and (b) absorption onset as a function of composition

3. Conclusions

Through substitution with the ethylenediammonium cation, we have probed the structure-composition-property relationship in the $(CH_3NH_3)_{1-2x}(H_3NC_2H_4NH_3)_xPbI_3$ system. Increasing the $(H_3NC_2H_4NH_3)^{2+}$ content leads to an evolution of unit cell parameters, absorption, photoluminescence and HOMO level, which provide experimental evidence for the creation of cation vacancies in the crystal structure and for the ability to tune the properties of the perovskite by control of the cation stoichiometry on the A site. Despite the importance of vacancies in inorganic oxides, the incorporation of defects (such as anion or cation vacancies) remains under explored in organic-inorganic tri-halide perovskites and this is something that could be explored more widely.

4. Experimental Section

Synthesis of bulk materials: CH_3NH_3I was prepared following literature methods.[58] The same procedure was used for the synthesis of $H_3NC_2H_4NH_3I_2$, replacing CH_3NH_2 with $H_2NC_2H_4NH_2$. The ammonium salts were recrystallized using ethanol and diethylether, filtered and then dried at 60 °C in a vacuum oven overnight. To synthesise $(CH_3NH_3)_{1-2x}(H_3NC_2H_4NH_3)_xPbI_3$ a procedure based on the method by Poglitsch *et al.* was used.[50] $Pb(Ac)_2 \bullet 3H_2O$ was dissolved in HI (57 wt%, stabilised with 1.5% H_3PO_2) at 100 °C. In a separate vial stoichiometric quantities of CH_3NH_3I and $H_3NC_2H_4NH_3I_2$ were dissolved in H_2O . The resulting solution was heated to 100 °C and to this solution, the lead solution, was added. The reaction was left overnight at 75 °C on a hotplate. The resulting crystals were filtered, washed with toluene and dried in an oven at 90 °C.

Film preparation: ITO coated substrates were used for photophysical measurements and were prepared by sequential sonication in Helmanex solution, deionised water, acetone, and then isopropanol, before being plasma ashed for 3 minutes at maximum power. Spin coating was carried out in a nitrogen filled glovebox with < 1 ppm O_2 and H_2O. The solution was spin coated at 500 RPM for 7 seconds and then 3000 RPM for 90 seconds, with chloroform being dropped on the film after 45 seconds at 3000 RPM. Samples were then annealed on a hotplate at 90 °C for 10 minutes inside the glovebox.

For photoluminescence and air photoemission measurements, thin films of $(CH_3NH_3)_{1-2x}(H_3NC_2H_4NH_3)_xPbI_3$ were synthesised by using two precursor solutions. Solutions were made by dissolving PbI_2, methylammonium iodide, ethylenediammonium iodide in DMSO in a 1:1 molar ratio to make a 0.6 M solution. The first solution was 1:0.6:0.2 of PbI_2:CH_3NH_3I:$H_3NC_2H_4NH_3I_2$ and the second solution was 1:1 PbI_2 to CH_3NH_3I. Samples of any substitution level between 0 and 20% $H_3NC_2H_4NH_3I_2$ could then be made with linear combinations of the two solutions.

Characterisation: Powder X-ray diffraction (PXRD) data were collected on a Panalytical Emperyean Diffractometer with a Ge (110) monochromator and Cu$K\alpha_1$ (λ=1.5406 Å) radiation. Data were collected in the region 5-100° 2 theta with a step size of 0.017 ° and a time per step of 1.3 s. Powder diffraction data was analysed using GSAS.[59, 60]

Density measurements were carried out on a Micromeritics AccuPyc 1340 Helium Gas Pycnometer.

Absorption Measurements were recorded in the solid phase, as a thin film (of ~150 nm thickness) a CARY 300 spectrophotometer at a scan rate of 100 nm/min with a background measurement taken to compensate for the absorption of glass.

Photoluminescence measurements were taken by exciting with 355 nm pulsed laser light generated by a Q-switched Nd:YAG laser. The pulses had a duration of ~5 ns and a repetition rate of 20 Hz. The Photoluminescence was coupled *via* fiber optic cable to an Ocean Optics USB4000 spectrometer.

Air photoemission measurements were obtained using a KP technology APS03 setup, with the samples being grounded via their ITO substrates in order to prevent charging effects. All samples were stored in a desiccator until immediately prior to use.

Acknowledgements

We acknowledge support by the Engineering and Physical Sciences Research Council (grant codes EP/M506631/1, EP/K015540/01, EP/K022237/1 and EP/M025330/1). IDWS and JTSI acknowledge Royal Society Wolfson research merit awards

References

1. A. Kojima, K. Teshima, Y. Shirai and T. Miyasaka, *J. Am. Chem. Soc.*, 2009, **131**, 6050-6051.
2. https://www.nrel.gov/pv/assets/images/efficiency-chart.png, (accessed 5th October 2017).
3. S. D. Stranks and H. J. Snaith, *Nat. Nanotechnol.*, 2015, **10**, 391-402.
4. N. J. Jeon, J. H. Noh, W. S. Yang, Y. C. Kim, S. Ryu, J. Seo and S. I. Seok, *Nature*, 2015, **517**, 476-480.
5. N. J. Jeon, J. H. Noh, Y. C. Kim, W. S. Yang, S. Ryu and S. Il Seol, *Nat. Mater.*, 2014, **13**, 897-903.

6. J. Burschka, N. Pellet, S.-J. Moon, R. Humphry-Baker, P. Gao, M. K. Nazeeruddin and M. Gratzel, *Nature*, 2013, **499**, 316-319.
7. M. Liu, M. B. Johnston and H. J. Snaith, *Nature*, 2013, **501**, 395-398.
8. G. E. Eperon, V. M. Burlakov, P. Docampo, A. Goriely and H. J. Snaith, *Adv. Funct. Mater.*, 2014, **24**, 151-157.
9. J. M. Ball, M. M. Lee, A. Hey and H. J. Snaith, *Energy Environ. Sci.*, 2013, **6**, 1739-1743.
10. M. M. Lee, J. Teuscher, T. Miyasaka, T. N. Murakami and H. J. Snaith, *Science*, 2012, **338**, 643-647.
11. L. Etgar, P. Gao, Z. Xue, Q. Peng, A. K. Chandiran, B. Liu, M. K. Nazeeruddin and M. Gratzel, *J. Am. Chem. Soc.*, 2012, **134**, 17396-17399.
12. A. Mei, X. Li, L. Liu, Z. Ku, T. Liu, Y. Rong, M. Xu, M. Hu, J. Chen, Y. Yang, M. Gratzel and H. Han, *Science*, 2014, **345**, 295-298.
13. S. D. Stranks, G. E. Eperon, G. Grancini, C. Menelaou, M. J. P. Alcocer, T. Leijtens, L. M. Herz, A. Petrozza and H. J. Snaith, *Science*, 2013, **342**, 341-344.
14. G. Xing, N. Mathews, S. Sun, S. S. Lim, Y. M. Lam, M. Graetzel, S. Mhaisalkar and T. C. Sum, *Science*, 2013, **342**, 344-347.
15. G. E. Eperon, S. D. Stranks, C. Menelaou, M. B. Johnston, L. M. Herz and H. J. Snaith, *Energy Environ. Sci.*, 2014, **7**, 982-988.
16. Y. Kawamura, H. Mashiyama and K. Hasebe, *J. Phys. Soc. Jpn*, 2002, **71**, 1694-1697.
17. P. S. Whitfield, N. Herron, W. E. Guise, K. Page, Y. Q. Cheng, I. Milas and M. K. Crawford, *Sci. Rep.*, 2016, **6**, 35685.
18. W. S. Yang, J. H. Noh, N. J. Jeon, Y. C. Kim, S. Ryu, J. Seo and S. I. Seok, *Science*, 2015, **348**, 1234-1237.
19. T. J. Jacobsson, J.-P. Correa-Baen, M. Pazoki, M. Saliba, K. Schenk, M. Gratzel and A. Hagfeldt, *Energy Environ. Sci.*, 2016, **9**, 1706-1724.
20. D. P. McMeekin, G. Sadoughi, W. Rehman, G. E. Eperon, M. Saliba, M. T. Hoerantner, A. Haghighirad, N. Sakai, L. Korte, B. Rech, M. B. Johnston, L. M. Herz and H. J. Snaith, *Science*, 2016, **351**, 151-155.
21. H. Choi, J. Jeong, H.-B. Kim, S. Kim, B. Walker, G.-H. Kim and J. Y. Kim, *Nano Energy*, 2014, **7**, 80-85.
22. F. Hao, C. C. Stoumpos, R. P. H. Chang and M. G. Kanatzidis, *J. Am. Chem. Soc.*, 2014, **136**, 8094-8099.
23. F. Hao, C. C. Stoumpos, C. Duyen Hanh, R. P. H. Chang and M. G. Kanatzidis, *Nat. Photonics*, 2014, **8**, 489-494.
24. J. Navas, A. Sanchez-Coronilla, J. Jesus Gallardo, N. Cruz Hernandez, J. Carlos Pinero, R. Alcantara, C. Fernandez-Lorenzo, D. M. De los Santos, T. Aguilar and J. Martin-Calleja, *Nanoscale*, 2015, **7**, 6216-6229.
25. S. Nagane, U. Bansode, O. Game, S. Chhatre and S. Ogale, *Chem. Commun.*, 2014, **50**, 9741-9744.
26. G. E. Eperon, T. Leijtens, K. A. Bush, R. Prasanna, T. Green, J. Tse-Wei Wang, D. P. McMeekin, G. Volonakis, R. L. Milot, J. B. Patel, E. S. Parrot, R. J. Sutton, W. Ma, F. Moghadam, B. Conings, A. Babayigit, H.-G. Boyen, S. Bent, F. Giustino, L. M. Herz, M. B. Johnston, M. D. McGehee and H. J. Snaith, *Science*, 2016, **354**, 861-865.
27. C. Yi, J. Luo, S. Meloni, A. Boziki, N. Ashari-Astani, C. Gratzel, S. M. Zakeeruddin, U. Roethlisbeger and M. Gratzel, *Energy Environ. Sci.*, 2016, **9**, 656-662.
28. M. Saliba, T. Matsui, J.-Y. Seo, K. Domanski, J.-P. Correa-Baena, M. K. Nazeeruddin, S. M. Zakeeruddin, W. Tress, A. Abate, A. Hagfeldt and M. Grätzel, *Energy Environ. Sci.*, 2016, **9**, 1989-1997.
29. B. Saparov and D. B. Mitzi, *Chem. Rev.*, 2016, **116**, 4558-4596.
30. D. B. Mitzi, *J. Mater. Chem.*, 2004, **14**, 2355-2365.
31. J. A. Hill, A. L. Thompson and A. L. Goodwin, *J. Am. Chem. Soc.*, 2016, **138**, 5886-5896.
32. P. Jain, N. S. Dalal, B. H. Toby, H. W. Kroto and A. K. Cheetham, *J. Am. Chem. Soc.*, 2008, **130**, 10450-10451.
33. H. J. Snaith, A. Abate, J. M. Ball, G. E. Eperon, T. Leijtens, N. K. Noel, S. D. Stranks, J. T.-W. Wang, K. Wojciechowski and W. Zhang, *J. Phys. Chem. Lett.*, 2014, **5**, 1511-1515.
34. C. Eames, J. M. Frost, P. R. F. Barnes, B. C. O'Regan, A. Walsh and M. S. Islam, *Nat. Commun.*, 2015, **6**.
35. P. Calado, A. M. Telford, D. Bryant, X. E. Li, J. Nelson, B. C. O'Regan and P. R. F. Barnes, *Nat. Commun.*, 2016, **7**.
36. H. Lee, S. Gaiaschi, P. Chapon, A. Marronnier, J. C. Vanel, D. Tondelier, J. E. Bouree, Y. Bonnassieux and B. Geffroy, *ACS Energy Letters*, 2017, **2**, 943-949.
37. I. Levine, P. K. Nayak, J. T. W. Wang, N. Sakai, S. Van Reenen, T. M. Brenner, S. Mukhopadhyay, H. J. Snaith, G. Hodes and D. Cahen, *J. Phys. Chem. C*, 2016, **120**, 16399-16411.
38. Z. Li, C. X. Xiao, Y. Yang, S. P. Harvey, D. H. Kim, J. A. Christians, M. J. Yang, P. Schulz, S. U. Nanayakkara, C. S. Jiang, J. M. Luther, J. J. Berry, M. C. Beard, M. M. Al-Jassim and K. Zhu, *Energy Environ. Sci.*, 2017, **10**, 1234-1242.
39. S. Stramare, V. Thangadurai and W. Weppner, *Chem. Mater.*, 2003, **15**, 3974-3990.
40. J. C. Boivin and G. Mairesse, *Chem. Mater.*, 1998, **10**, 2870-2888.
41. Y. Zhao and L. L. Daemen, *J. Am. Chem. Soc.*, 2012, **134**, 15042-15047.
42. S. Meloni, T. Moehl, W. Tress, M. Franckevicius, M. Saliba, Y. H. Lee, P. Gao, M. K. Nazeeruddin, S. M. Zakeeruddin, U. Rothlisberger and M. Gratzel, *Nat. Commun.*, 2016, **7**.
43. A. Walsh, D. O. Scanlon, S. Chen, X. G. Gong and S.-H. Wei, *Angew. Chem. Int. Ed.*, 2015, **54**, 1791-1794.
44. T.-Y. Yang, G. Gregori, N. Pellet, M. Gratzel and J. Maier, *Angew. Chem. Int. Ed.*, 2015, **54**, 7905-7910.
45. G. E. Eperon, C. E. Beck and H. J. Snaith, *Materials Horizons*, 2016, **3**, 63-71.
46. Z. Zhou, S. Pang, F. Ji, B. Zhang and G. Cui, *Chem. Commun.*, 2016, **52**, 3828-3831.
47. W. J. Ke, C. C. Stoumpos, I. Spanopoulos, L. Mao, M. Chen, M. R. Wasielewski and M. G. Kanatzidis, *J. Am. Chem. Soc.*, 2017, **139**, 14800-14806.
48. W. J. Ke, C. C. Stoumpos, M. H. Zhu, L. L. Mao, I. Spanopoulos, J. Liu, O. Y. Kontsevoi, M. Chen, D. Sarma, Y. B. Zhang, M. R. Wasielewski and M. G. Kanatzidis, *Sci. Adv.*, 2017, **3**.
49. A. Fraccarollo, L. Marchese and M. Cossi, *J. Phys. Chem. C*, 2018, **122**, 3677-3689.
50. A. Poglitsch and D. Weber, *J. Chem. Phys.*, 1987, **87**, 6373-6378.
51. J. L. Payne, C. Ni, L. Krishnan Jagadamma, J. R. Harwell, I. D. W. Samuel and J. T. S. Irvine, *in preparation*, 2018.
52. P. Schulz, E. Edri, S. Kirmayer, G. Hodes, D. Cahen and A. Kahn, *Energy Environ. Sci.*, 2014, **7**, 1377-1381.
53. Q. Chen, N. De Marco, Y. Yang, T. B. Song, C. C. Chen, H. X. Zhao, Z. R. Hong and H. P. Zhou, *Nano Today*, 2015, **10**, 355-396.
54. P. Umari, E. Mosconi and F. De Angelis, *Sci. Rep.*, 2014, **4**.
55. M. R. Filip, G. E. Eperon, H. J. Snaith and F. Giustino, *Nat. Commun.*, 2014, **5**.

56. A. Amat, E. Mosconi, E. Ronca, C. Quarti, P. Umari, M. K. Nazeeruddin, M. Gratzel and F. De Angelis, *Nano Lett.*, 2014, **14**, 3608-3616.
57. J. H. Lee, N. C. Bristowe, S. H. Lee, P. D. Bristowe, A. K. Cheetham and H. M. Jang, *Chem. Mater.*, 2016, **28**, 4259-4266.
58. H. Zhou, Q. Chen, G. Li, S. Luo, T.-b. Song, H.-S. Duan, Z. Hong, J. You, Y. Liu and Y. Yang, *Science*, 2014, **345**, 542-546.
59. B. H. Toby, *J. Appl. Crystallogr.*, 2001, **34**, 210-213.
60. A. C. Larson and R. B. von Dreele, *General Structure Analysis System (GSAS)*, Los Alamos National Laboratory Report, 2004.

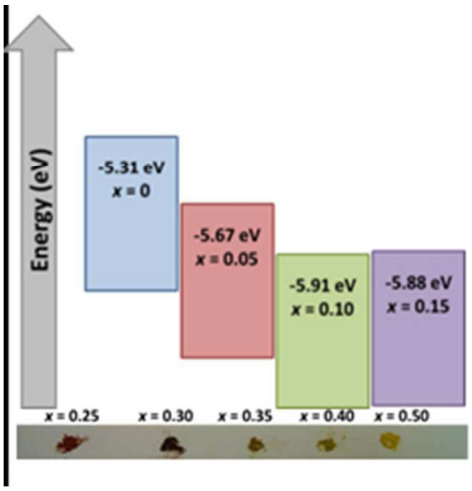

40x40mm (150 x 150 DPI)